J. Fluid Mech. (1969), *vol.* 36, *part* 2, *pp.* 309–335
Printed in Great Britain

A study of Bénard convection with and without rotation

By H. T. ROSSBY†
Department of Meteorology
Massachusetts Institute of Technology

(Received 16 May 1968 and in revised form 2 October 1968)

An experimental study of the response of a thin uniformly heated rotating layer of fluid is presented. It is shown that the stability of the fluid depends strongly upon the three parameters that described its state, namely the Rayleigh number, the Taylor number and the Prandtl number. For the two Prandtl numbers considered, 6·8 and 0·025 corresponding to water and mercury, linear theory is insufficient to fully describe their stability properties. For water, subcritical instability will occur for all Taylor numbers greater than 5×10^4, whereas mercury exhibits a subcritical instability only for finite Taylor numbers less than 10^5. At all other Taylor numbers there is good agreement between linear theory and experiment.

The heat flux in these two fluids has been measured over a wide range of Rayleigh and Taylor numbers. Generally, much higher Nusselt numbers are found with water than with mercury. In water, at any Rayleigh number greater than 10^4, it is found that the Nusselt number will increase by about 10 % as the Taylor number is increased from zero to a certain value, which depends on the Rayleigh number. It is suggested that this increase in the heat flux results from a perturbation of the velocity boundary layer with an 'Ekman-layer-like' profile in such a way that the scale of boundary layer is reduced. In mercury, on the other hand, the heat flux decreases monotonically with increasing Taylor number. Over a range of Rayleigh numbers (at large Taylor numbers) oscillatory convection is preferred although it is inefficient at transporting heat. Above a certain Rayleigh number, less than the critical value for steady convection according to linear theory, the heat flux increases more rapidly and the convection becomes increasingly irregular as is shown by the temperature fluctuations at a point in the fluid.

Photographs of the convective flow in a silicone oil (Prandtl number = 100) at various rotation rates are shown. From these a rough estimate is obtained of the dominant horizontal convective scale as a function of the Rayleigh and Taylor numbers.

1. Introduction

This experimental study is concerned with the response of a thin horizontal layer of fluid rotating about the vertical axis when it is subject to uniform heating from below and cooling from above. In general, the unstable stratification will cause convective motions whenever the temperature difference exceeds

† Present address: Department of Geology and Geophysics, Yale University.

a certain minimum value, which depends on the fluid, the rate of rotation and the boundary conditions.

It can be shown that within the meaning of the Boussinesq approximation (Spiegel & Veronis 1960) the state of this fluid-dynamical system is completely defined by three parameters, namely the Rayleigh number

$$R = \alpha g \Delta T d^3/\nu\kappa, \tag{1.1}$$

the Taylor number

$$Ta = 4\Omega^2 d^4/\nu^2 \tag{1.2}$$

and the Prandtl number

$$P = \nu/\kappa, \tag{1.3}$$

where α is the coefficient of thermal expansion, g is the gravitational acceleration, ΔT and d are respectively the temperature difference and depth across the fluid, ν and κ are respectively the coefficients of viscous and thermal diffusivity and Ω is the rate of rotation about the vertical axis. The Rayleigh number represents in non-dimensional form the amount of potential energy being applied to the fluid and the Taylor number is a measure of the rotation rate. The Prandtl number clearly is a function of the parameters of the fluid only.

Whenever the Rayleigh number is greater than a certain minimum value convection will occur. If the Taylor number is zero, this critical Rayleigh number is independent of the Prandtl number and depends only on the boundary conditions. For obvious reasons we will limit our discussion to apply only to rigid boundaries at the top and the bottom.

When the fluid is rotated, the critical Rayleigh number becomes a complex function of both the Taylor and the Prandtl numbers. Thus, according to linear stability theory (Chandrasekhar 1961), at any arbitrary Prandtl number greater than unity instability will result in steady motions at a Rayleigh number which depends only on the Taylor number. At small Prandtl numbers, however, instability may result in either steady or oscillatory motions depending on *both* the Prandtl *and* the Taylor numbers. Both types of instabilities have been confirmed experimentally by Fultz & Nakagawa (1955) and Nakagawa & Frenzen (1955).

Recently Veronis (1959, 1966) has indicated the possibility of a finite-amplitude instability at subcritical Rayleigh numbers over a certain range of Taylor numbers provided the Prandtl number is less than $\sqrt{2}$. This instability was not observed in either of the two experimental studies mentioned above.

The first part of this study was therefore an effort to establish experimentally the relationship between the critical Rayleigh number and the Taylor number in two different fluids, namely water and mercury. Does mercury ($P = 0{\cdot}025$) exhibit this finite-amplitude instability? How good is the agreement between experiment and theory? According to the analysis of Veronis, water should not exhibit this instability. Is this true?

The second objective of this study was to explore how the heat flux, once convection is established, depends on both the Rayleigh number and the Taylor numbers in mercury and water. For the special case of no rotation, however, the heat flux in three fluids, mercury, water and a silicone oil ($P \sim 200$), will be discussed separately.

The next section (2) discusses the details of the experimental approach. The

following section (3) reviews briefly some attempts to explore the structure of the flow photographically. Sections 4 and 5 respectively discuss the results of the heat flux measurements without and with rotation.

2. The convection apparatus

The fluid under study was contained between two essentially symmetric blocks stacked face to face in the vertical (see figure 1). Each one consisted of a solid aluminium cylinder $8\frac{3}{4}$ in. in diameter and 4 in. high and an $8\frac{3}{4}$ in. $\times \frac{1}{2}$ in. thick copper disk, which were held together by a thick epoxy bond. Thus the fluid was sandwiched between the two copper disks. The Rayleigh number was computed from the temperature difference across the fluid and the heat flux was computed from the temperature drop across the epoxy layers. A discussion of this is given in appendix A. The cooling of the upper block was arranged by milling a double spiral groove ($\frac{1}{2}$ in. $\times \frac{1}{2}$ in. cross-section) into the top flat surface for the thermostated cold water circulation. A 1·4 in. aluminium lid was screwed on to seal in the spiral groove. Two $\frac{1}{2}$ in. pipes were added diametrically opposite each other on the sides to connect the hosing to the cooling spiral.

The aluminium surfaces to be bonded to the copper disks were flycut flat to 0·001 in. and the latter were ground plane parallel in a Blanchard grinder to less than 0·001 in.

Nine $\frac{1}{16}$ in. (36 in all) holes for thermocouples were drilled in both aluminium blocks and each copper plate. The end of these holes defined a 3×3 grid pattern with 2 in. spacing in a flat plane $\frac{1}{4}$ in. from the surfaces to be bonded (see figure 2). To fill and empty the convection chamber, a pipe on the side of each copper disk had access to it through a small hole $\frac{1}{2}$ in. from the perimeter. The copper disks were chromium-plated to prevent oxidation or amalgamation.

The crucial step in the assembly was the bonding of the copper disks to the aluminium cylinders. If the former are to have a constant temperature it is essential that the bond be firm and uniform. To achieve this the surfaces to be bonded were carefully cleaned. Then a $\sim 0{\cdot}3$ in. layer of epoxy was bonded on each of the aluminium surfaces. When hardened, the epoxy layers were machined to exactly the same thickness and flat to $< 0{\cdot}001$ in. The copper plates were bonded to these layers with another epoxy of low viscosity to ensure good flow when they were pressed together. For the mercury heat flux measurements the epoxy was replaced with graphite with a higher thermal conductivity. This permitted a larger flux and hence larger temperature gradients across the mercury without heating and cooling the aluminium blocks excessively.

Electric wiring

The temperature difference between the copper plates and aluminium blocks respectively were measured by two nine-unit thermopiles, T_{32} and T_{41}, each junction occupying one hole in the copper or the aluminium. T_{32} and T_{41} respectively measure the temperature difference between the copper plates and the aluminium blocks. The junctions were electrically insulated with nail polish. Good thermal contact was obtained by filling the holes with a paste of

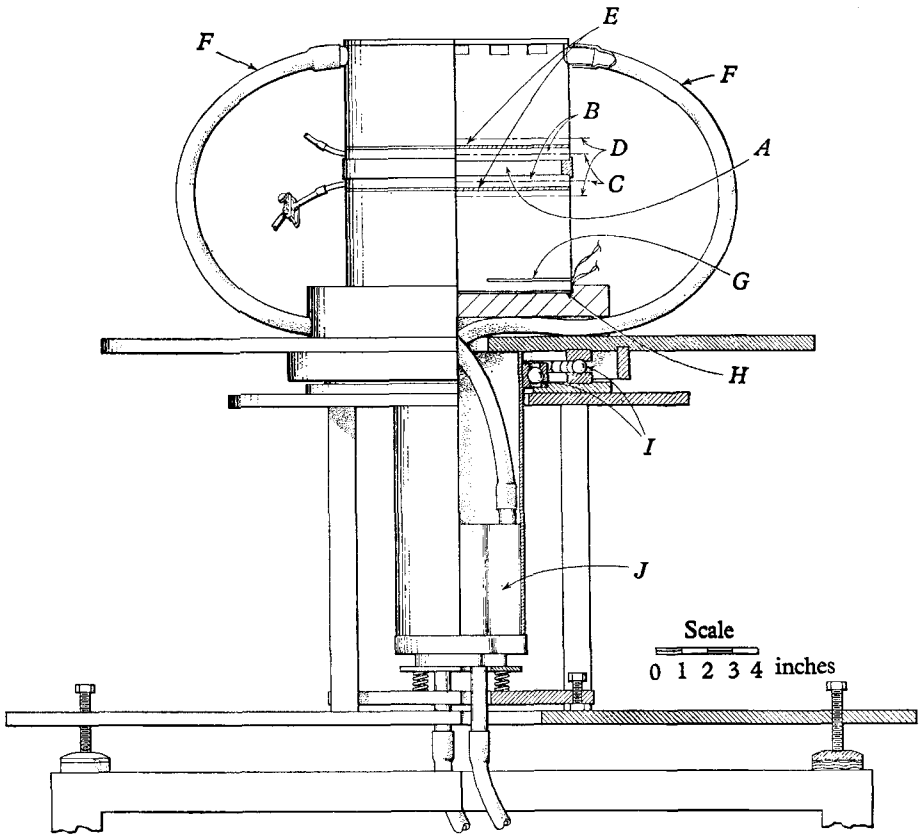

FIGURE 1. View of the experimental apparatus centred on the rotating table. During experiments it was thermally protected with cotton insulation. *A*, convection chamber; *B*, copper plates; *C*, thermopile T_{32} which measures the temperature difference between the copper plates; *D*, thermopile T_{41} which measures the temperature difference between the aluminium blocks; *E*, epoxy layers used to measure heat flux; *F*, thermostated cold water circulation; *G*, thermistor probe used to control temperature of lower aluminium block; *H*, electric heating pad; *I*, thrust and radial bearings; *J*, 'fluid slip rings' (see text). Not shown are any of the electric slip rings or the motor to control the rotation of the table.

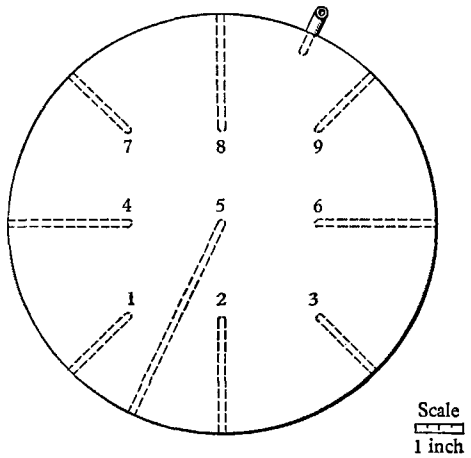

FIGURE 2. Planform of the thermocouples in the copper plates and the aluminium blocks.

aluminium oxide. The outputs from the two thermopiles were brought out from the rotating table through high-quality electric slip rings. The maximum spurious e.m.f. summed over all connectors and slip rings was less than 1 μV, which corresponds to $\approx 1/360$ °C. The procedure for taking the measurements and computing the non-dimensional parameters is discussed in appendix A.

Two additional thermocouples were arranged in such a way that the mean temperature of the copper disks, and hence of the fluid, was known.

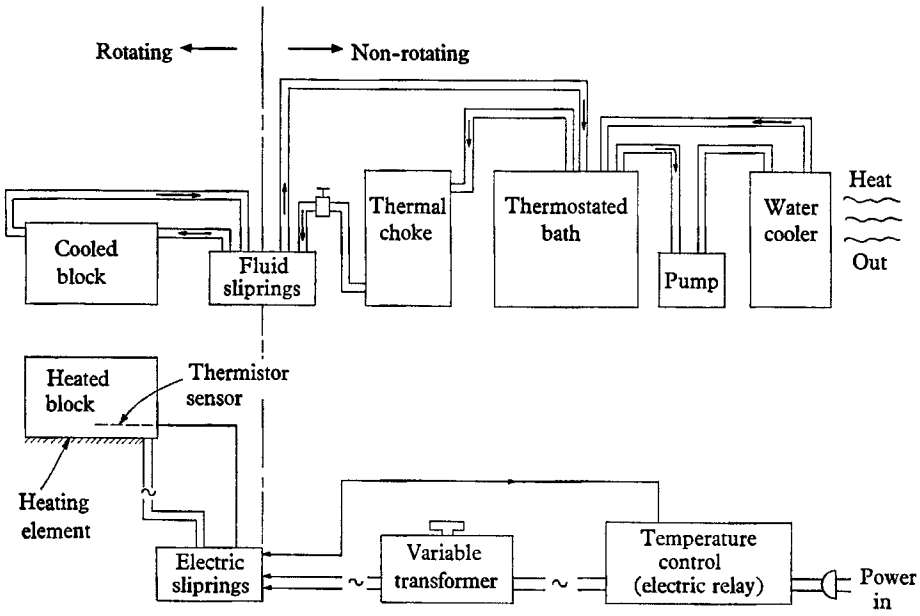

FIGURE 3. Schematic diagram of the heating and cooling systems.

The lower block was heated electrically by a rubber-insulated bifilar wound circular heating pad ($8\frac{3}{4}$ in. $\times \frac{1}{16}$ in.) bonded directly to the bottom surface of the lower block. The maximum thermal dissipation was 360 W. The thermistor probe, which regulated the temperature of the lower block, was placed $\frac{3}{8}$ in. above the heating pad in a 3 in. deep hole.

The thermostating system

The power to the heating pad was regulated by a Fisher model 44 temperature control using the thermistor probe as its sensor (see figure 3). The voltage was stepped down from 117 Va.c. to 0–60 Va.c. by a variable voltage transformer in order to obtain an optimum heating rate.

The thermostated cold water was regulated by a Haake thermostated bath and was steady to $\pm 0{\cdot}03$ °C. The circulation pump has both pressure and suction, so that the mean pressure of the circulated water was close to atmospheric pressure, thus reducing the risk of leakage in the fluid slip rings (see below). After the water left the thermostated bath it passed through a thermal choke. The heat was eliminated from the bath by an independent closed-circuit

water circulation using a standard drinking fountain water cooler. The temperature difference between the aluminium blocks, as measured by the thermopile, was steady to $\pm 0{\cdot}005$ °C.

The rotating table and drive

The apparatus rests on a large formica block centred on a $\frac{1}{2}$ in. thick steel plate of 30 in. diameter, which is supported by one thrust bearing and one axial bearing (diameters 11 in. and 6 in.). A 5 in. diameter shaft descends below the table on the inside of the bearings and serves two purposes. On its outside a formica sleeve with six silver slip rings is attached. Three brushes rest against each ring to ensure adequate electrical contact. Two of these are used for the electric heating pad and two for the thermistor probe.

Inside the shaft is mounted a two-channel fluid slip ring system for transferring the thermostated cold water to and from the rotating framework. The central stationary core is made of formica and the rotating seal rings are supported by a lucite cylinder which fits snugly over the core.

The turntable was driven by a $\frac{1}{4}$ h.p. motor mounted on a separate frame with a variable-speed transmission with an output ranging from 0 to 360 rev/min. The torque was applied to the turntable by a timing belt and two pulleys of 2 in. and 14 in. diameters, giving a speed reduction of $7\times$. On the motor-shaft a small flywheel was added to improve the stability of the transmission, particularly at low speeds. A tachometer was run off the flywheel to check the stability of the rotation. The peak-to-peak variation of the table's rotation (including drift) was less than 1 % for rotation periods ~ 100–300 sec, improved to 0·4 % at 40 sec, and levelled off to $< 0{\cdot}3$ % for shorter periods.

3. Visual studies of thermal convection with and without rotation

It is instructive to have some feeling for the spatial structure of the convective flow for different values of Rayleigh and Taylor numbers. For example, when is the flow laminar, when turbulent, and, particularly, how is it modified as the rotation is increased? The following photographs were taken with these questions in mind.

The technique for visualizing the flow is to illuminate a suspension of aluminium powder in the fluid with a collimated beam of light. The background was kept dark to improve the contrast. With long time exposures the bright particles would generate streaks as they moved with the fluid. A fluid with a moderately high viscosity, a 10 cSt silicone oil with a Prandtl number 100, was used so that the particles would remain in suspension for the duration of the experiment. A few photographs are presented in figures 4–6, plates 1, 2 and 3, which give a vertical view of the horizontal structure. The photographs of the fluid were taken through a hollow glass lid through which constant-temperature thermostated water is circulated. Information on the photographs is given in tables 1, 2 and 3, where ΔT is the temperature difference across the fluid, Ω is the rotation rate in radians per second, s is the non-dimensional wavelength, $T_{\exp}$ is the exposure time of the photograph and r is defined in equation (3.2).

The following paragraphs give a discussion of some of the more outstanding features in the photographs.

(i) From these and other photographs rolls and roll-like cells appear to be the preferred mode of convection from at least $R = 2200$ to at least $R = 87{,}000$ when there is no rotation. This does not exclude the existence of squares or hexagons near the critical Rayleigh number.

(ii) At a certain Rayleigh number between 11,000 and 26,000 without rotation the rolls lose their strict two-dimensional form to include a lengthwise periodic triangular structure. This pattern appears to be stable up to Rayleigh numbers of $O(10^5)$ or more, depending on the Prandtl number. The physical mechanism for this instability is not clear to the writer. Recently, Busse (1966) investigated the stability of two-dimensional rolls at large R and has found that they become unstable at $R = 22{,}000$, which is consistent with these observations.

(iii) At higher Rayleigh numbers the basic cell pattern becomes less distinct (figure 6(*a*), plate 3), and, although it may be stable with respect to the convective time scale (depending on the Prandtl number), it does drift about over long periods of time. This has been verified with a time-lapse film study.

(iv) When the fluid is rotated rapidly, a transition takes place at a certain radius beyond which the rolls are radially oriented (see figure 4(*b*), (*d*), (*f*), plate 1). The mechanism for this is clear. When the apparatus is rotated, a radial acceleration, which increases with radius, is established. The dark lines in the photographs represent zones of rising warm and sinking cold fluid alternately. If the radial acceleration and the density difference is large enough, a ring of cold fluid will be unstable with respect to a ring of warm fluid just outside it and will attempt to replace it. If this were to happen, however, the cold ring would become unstable with respect to the next ring of warm fluid, and so on. The only stable orientation for the rolls is radial, in which case the radial acceleration is perpendicular to the thermal field.

A very crude estimate of the critical radius may be obtained by computing a Rayleigh number associated with the radial acceleration $\Omega^2 r$. If we assume that the temperature difference between adjacent rolls is $\sim \frac{1}{2}\Delta T$, the horizontal scale is $\frac{1}{2}sd$ and a critical Rayleigh number, R_c, for the twisting of a roll is ~ 500, roughly corresponding to the critical Rayleigh number with free boundary conditions, we have

$$R_c \sim \frac{\alpha\Omega^2 r\Delta T\,(\frac{1}{2}sd)^3}{2\nu\chi} = R(\tfrac{1}{2}s)^3\frac{\Omega^2 r}{2g} \sim 500, \tag{3.1}$$

where R is the imposed Rayleigh number. We find the critical radius is

$$r \simeq 10^3\frac{g}{\Omega^2 R}(2/s)^3. \tag{3.2}$$

Estimates of r are given in tables 1–3. The agreement is consistent insofar as the instability appears in figures 4(*b*), (*d*) and (*f*), where in fact r is smaller than the radius of the container (10 cm), although according to (3.2) we should observe this instability in figure 5(*f*) also. However, since this radial acceleration destroys the horizontal uniformity, which is a basic assumption in the Bénard

convection problem, it is essential that its influence be minimized. Obviously the radical acceleration cannot be eliminated entirely.

(v) In figures 5(*d*), (*f*) and 6(*c*), (*d*) one observes a buckling of the rolls without any particular orientation. As the rotation is further increased they break up into cyclonic and anticyclonic vortices. Presumably the buckling is

	R	Ta	ΔT	Ω	s	T_{exp}	r
4(*a*)	10,300	0	3·2	0	2·1	60	—
4(*b*)	10,300	1400	3·2	3·92	1·9	20	7
4(*c*)	26,000	0	7·9	0	2·8	15	—
4(*d*)	25,000	1060	7·8	3·43	2·1	15	3
4(*e*)	43,000	0	13·4	0	2·8	15	—
4(*f*)	42,000	1580	13·1	4·19	1·7	60	2

TABLE 1. Parameter values for photographs of thermal convection in figure 4. The Prandtl number is 100 and the depth is 0·7 cm

	R	Ta	ΔT	Ω	s	T_{exp}	r
5(*a*)	11,000	0	1·12	0	2·3	15	—
5(*b*)	11,000	2020	1·12	2·24	2·1	15	16
5(*c*)	35,000	0	3·5	0	2·7	60	—
5(*d*)	35,000	2020	3·5	2·24	1·7	15	9
5(*e*)	87,000	0	8·7	0	2·4	60	—
5(*f*)	84,000	1970	8·4	2·21	1·56	60	5

TABLE 2. Parameter values for photographs of thermal convection in figure 5. The Prandtl number is 100 and the depth is 1·0 cm

	R	Ta	ΔT	Ω	s	T_{exp}	r
6(*a*)	820,000	0	13·7	0	—	60	—
6(*b*)	800,000	100,000	13·4	4·83	—	5	—
6(*c*)	56,000	4,400	0·94	1·0	1·46	15	60
6(*d*)	37,000	11,000	0·62	1·57	1·54	15	23
6(*e*)	38,000	51,000	0·63	3·43	1·16	15	11
6(*f*)	57,000	90,000	0·96	4·5	—	15	—

TABLE 3. Parameter values for photographs of thermal convection in figure 6. The Prandtl number is 100 and the depth is 1·8 cm

some form of baroclinic instability. One can compare this with the non-axisymmetric flows that occur in the annulus experiments of Fowlis & Hide (1965). Their relevant parameters are

$$\theta = \frac{\alpha g \Delta T d}{\Omega^2 (b-a)^2}, \quad T = \frac{4\Omega^2 (b-a)^5}{\nu^2 d}, \tag{3.3}$$

where $(b-a)$ is the spacing of the annulus. Assuming a square cross-section for our rolls, we can then replace $(b-a)$ with d. For figure 6(*d*), for example, we find the values for these parameters to be $\theta = 0{\cdot}14$ and $T = 11{,}000$. The latter is an order of magnitude smaller than the value necessary for non-axisymmetric flows according to Fowlis & Hide (1965). This may be for two reasons: either

the comparison is invalid or the disparity is due to the different boundary conditions. Our system is inherently more unstable, since we are considering rolls which are free to move as a whole, not instabilities within a mechanically constrained convective cell as in the annulus experiment. The vortices that appear at higher Taylor numbers are very similar to those observed by Nakagawa & Frenzen (1955).

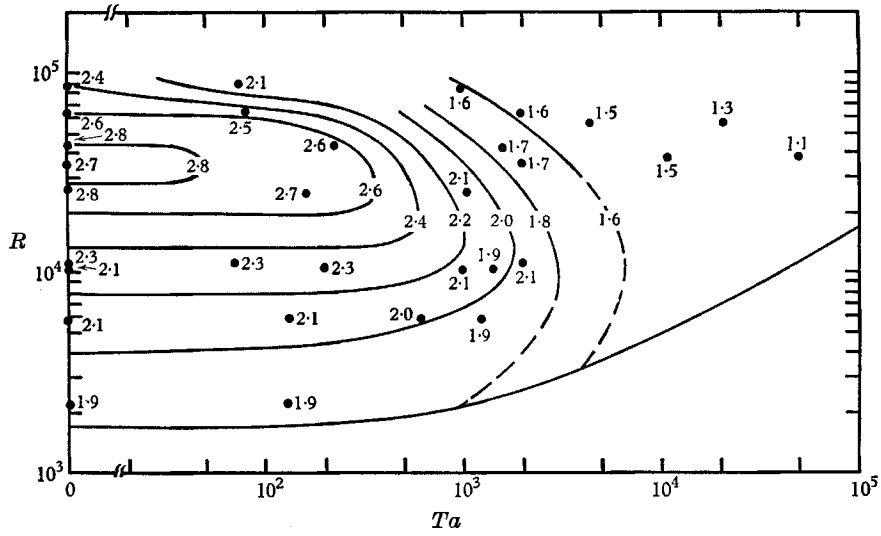

FIGURE 7. Lines of constant characteristic non-dimensional horizontal wavelength as a function of the Rayleigh and Taylor numbers.

In figure 7 we have attempted to summarize on the basis of these and other photographs the horizontal scale as a function of the Rayleigh and Taylor numbers. The dimensionless wavelength, which includes only the most pronounced horizontal scales, is defined as twice the horizontal scale divided by the depth.

4. The convective heat transfer in a stationary system

The principle objective of this study has been to carefully explore the character of the stability properties of the fluid as well as the magnitude of the convective heat transfer over a wide range in rotation rates. The particular case of no rotation, however, has been the subject of considerable study in the past and consequently it is convenient to consider the results pertaining to this case separately in more detail. We shall do this in this section and the results of the rotating experiments are presented in the next section. In all that follows the data will be presented, summarized and discussed in non-dimensional form. A detailed discussion on the non-dimensionalization of the experimental results is given in appendix A.

Three fluids were used in the heat flux measurements: a 20 cSt silicone oil (hereafter referred to as the oil), water and mercury, which cover a range in

Prandtl numbers from 200 to 0·025. The measured relationship between the Nusselt number and the Rayleigh number for these fluids is presented separately in figures 8–10. The experimentally obtained values for the critical Rayleigh number and the initial rate of increase of heat flux by convection (frequently known as the initial slope) by this study as well as several of the earlier investigations are summarized in table 4.

Study	d (cm)	ΔT (°C)	R_c	Initial slope	Fluid
Schmidt & Milverton	0·4	1·7	1970	1·76*	Water†
(1935)	0·45	1·0	1580	2·22*	Water†
	0·5	1·05	1850	1·78*	Water†
	0·55	0·84	1670	2·18*	Water†
Schmidt & Saunders	0·5	1·25	1800	1·89	Water†
(1938)	0·4	2·1	1700	2·12	Water†
Malkus‡ (1954)	0·508	0·741§	1780§‖	2·89	Water†
	1·016	—	—	2·74	Water†
Silveston (1958)	0·145	16·1	1820	2·25	Water
	0·305	3·29	1640¶	2·31¶	Water
	0·305	11·7	1750	2·45	Glycol (P = 135)
Present work	0·499	2·87	1810	2·50	20 cSt silicone oil (P = 200)
	0·499	0·86	1760	2·45	Water
	0·693	1·50	1680	1·28	Mercury

* Experiment not designed for accurate local flux measurement.
† Did not report values used for the physical properties.
‡ Non-steady experiment.
§ Estimated from published diagrams.
‖ Used data from appendix B.
¶ Insufficient data for accurate estimate (these are lower limits).

TABLE 4. Summary of various experimental results, including those of the present work, at the critical Rayleigh number

We have found very good overlap in the Nusselt numbers when obtained at the same Rayleigh number, but with different depths of the fluid. This is strong evidence that the heat flux measurements were done in an accurate and self-consistent manner. Except with mercury, where the scatter is somewhat larger, this overlap is within $\pm 2\,\%$.

However, very near the critical Rayleigh number there is a larger scatter in the results, as is evident in figures 9–10. This lack of uniqueness, as Koshmieder (1966) pointed out, is very likely associated with the sensitivity of the convective pattern to the shape of the container as well as the rate at which the equilibrium Rayleigh number is approached.

As in the past, the measured critical Rayleigh numbers are in reasonable agreement with theory. It is true that the discrepancies are larger than the error in measurement of the temperature differences across the fluid. However, we do not know the limits of accuracy of those physical properties upon which

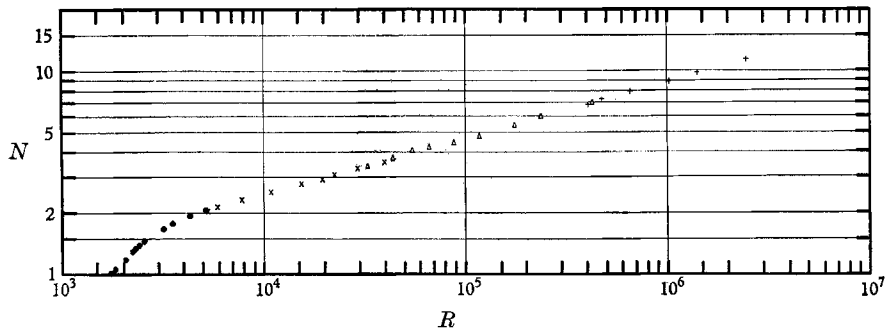

FIGURE 8. The Nusselt number as a function of the Rayleigh number in a silicone oil with Prandtl number 200. The depth of the fluid was: ●, 0·5 cm; ×, 1·0 cm; △, 2·0 cm; +, 3·5 cm.

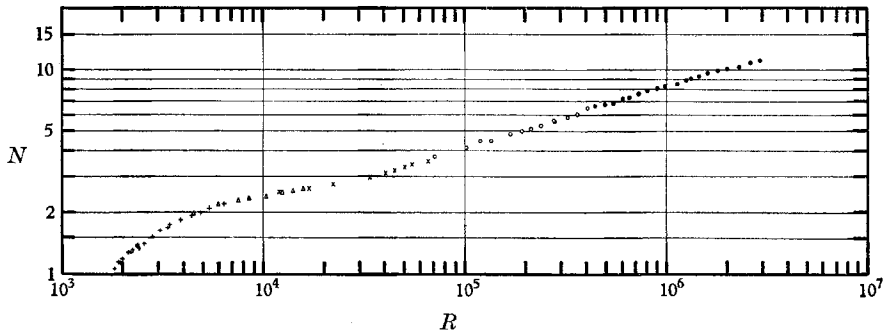

FIGURE 9. The Nusselt number as a function of the Rayleigh number in water with Prandtl number 6·8. The depth of the fluid was: +, 0·5 cm; △, 0·7 cm; ×, 1·0 cm; ○, 2·0 cm; ●, 3·5 cm.

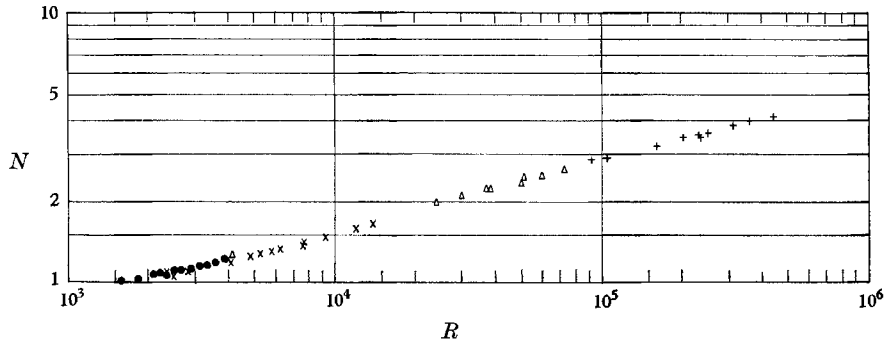

FIGURE 10. The Nusselt number as a function of the Rayleigh number in mercury with Prandtl number 0·025. The depth of the fluid was: ●, 0·69 cm; ×, 1·0 cm; △, 1·8 cm; +, 3·0 cm.

the Rayleigh number depends. For example, values for the thermal conductivity of water differ by 2 %. Silveston (1958) uses a value of the coefficient of thermal expansion which at 20 °C is 2·5 % smaller than ours. Published values for the thermal conductivity of mercury range from 0·017 to 0·023 cal/cm sec °C. The values that have been used in this study are all listed in appendix B. In fact, the ease with which one can measure the critical temperature difference suggests that it could be used as an independent method of measuring one of the physical properties, such as the heat capacity, provided the other relevant properties are known to sufficient accuracy.

Study	Results	Range in R	N (at $R=10^6$)	Fluid
Mull & Reiher† (1930)	$N = 0{\cdot}22R^{\frac{1}{4}}$	$0{\cdot}7\times10^4-2{\cdot}7\times10^5$	—	Air
	$N = 0{\cdot}075R^{\frac{1}{3}}$	$R > 2{\cdot}8\times10^5$	7·5	Air
Schmidt & Saunders (1938)	$N = 0{\cdot}098R^{0{\cdot}346}$	30,000–150,000	—	Water
Malkus (1954)	$N = 0{\cdot}186R^{0{\cdot}260\pm0{\cdot}004}$	$R < 500{,}000$	—	Water
	$N = 0{\cdot}085R^{0{\cdot}325\pm0{\cdot}005}$	$R > 500{,}000$	7·54	Acetone
Silveston (1958)	$N = 0{\cdot}24R^{\frac{1}{4}}$	4,000–44,000	—	Water
	$N = 0{\cdot}111R^{0{\cdot}31}$	$R > 25{,}000$	9·57	Water
Globe & Dropkin (1959)	$N = 0{\cdot}76R^{0{\cdot}2}$	$7\times10^6-3\times10^8$	12	Water
Present work	$N = 0{\cdot}184R^{0{\cdot}281\pm0{\cdot}005}$	$R > 4{,}000$	8·93	Silicone oil
	$N = 0{\cdot}131R^{0{\cdot}30\pm0{\cdot}005}$	$R > 34{,}000$	8·27	Water
	$N = 0{\cdot}147R^{0{\cdot}257\pm0{\cdot}004}$	$R > 20{,}000$	5·12	Mercury

† Taken from Jakob's (1946) interpretation of Mull & Reiher's (1930) study, assuming a Prandtl number of 0·72.

TABLE 5. Summary of various experimental results, including those of the present work, at large Rayleigh numbers

The initial slope for the rate of increase of the total heat flux just above the critical Rayleigh number is about the same for the oil and water and is in reasonable agreement with the value Silveston obtained with glycol. His smaller value for water, particularly with a fluid depth of only 0·145 cm (with a correspondingly large ΔT) is probably due to the large variation with temperature of the viscosity and the coefficient of expansion. The low values for the initial slopes obtained in earlier studies (except Malkus 1954) are probably due to inadequate compensation or correction of heat losses from their experimental apparatus.

The Nusselt numbers for the oil and water are in good agreement up to Rayleigh number of about 7000, beyond which the difference is almost certainly due to the influence of the relatively smaller Prandtl number for water.

We have approximated our results for the oil and water in three relations in table 5. The maximum deviation of any measurement from these relations is

about 4 %. The error is clearly not random, for there is a definite waviness in the Nusselt number data which may possibly be related to the discrete changes in the rate of increase of heat flux reported by Malkus (1954). By plotting the heat flux linearly against the Rayleigh number, one can identify these transitions somewhat better, but there appears to be little correspondence between these and those observed by Malkus. On the other hand, far too few measurements were made here to study adequately such a delicate feature.

Silveston's formula and ours for the Nusselt number at large R disagree (unlike the data) by 16 % at $R = 10^6$, which shows that one cannot expect to condense all the results into a single formula $N = f(R)g(P)$ correctly describing the role of *both* the Rayleigh *and* the Prandtl number. However, a detailed comparison of our results with Silveston's data shows very satisfactory agreement between his and our values for water and between his for glycol ($P = 135$) and ours for the oil ($P = 200$) at all measured Rayleigh numbers. We also point out that a detailed examination of Globe & Dropkin's (1959) data for water suggest that $N \propto R^{0.2}$, a relationship which has apparently gone unnoticed.

The results for mercury are quite different. We find the critical Rayleigh number to be 1680, but the initial slope is only 1·28, which is much smaller than the value at large Prandtl numbers. At large Rayleigh numbers (> 20,000) the data can be approximated by

$$N = 0{\cdot}147R^{0{\cdot}247 \pm 0{\cdot}004}. \tag{4.1}$$

This result is not consistent with that of Globe & Dropkin (1959), who obtained a $\frac{1}{3}$ law relation. It is true that our results extend only to $R = 500{,}000$, whereas their measurements start at $R = 180{,}000$. Nevertheless, in this small overlapping range the agreement is poor. At $R = 200{,}000$, for example, we have $N = 3{\cdot}4$ and Globe & Dropkin have 2·4. It is possible that the poor aspect ratios (diameter/depth) 2·5 and 0·5 in their apparatus contributed to the large error but it is more likely due to heat fluxes in the side walls, which have not been taken into account.

It appears that the flow in mercury is always turbulent and even within the thermal boundary layer we can expect large-amplitude velocity fluctuations. On the other hand, the high thermal conductivity of the fluid effectively limits the establishment of horizontal density gradients which are required to drive the convection. Hence, qualitatively, we see how it is not the viscosity but the conductivity that is limiting the convective heat transfer. Thus for finite-amplitude convection the controlling parameter is really PR rather than R. We do not use it, however, because it would confuse the diagrams to use the ordinary Rayleigh number near the critical value, where it is still the controlling parameter, and switch to PR at larger values.

The fact that mercury has a very small kinematic viscosity means that any convective flow is sensitive to shear instability. It is perhaps not surprising therefore that the flow should exhibit irregular temperature fluctuations even at only slightly supercritical Rayleigh numbers.

5. The convective heat transfer in a rotating system

The convective heat transfer in water and mercury has been measured over a wide range in Rayleigh and Taylor numbers, which includes the limit of no convection (or marginal stability). The two fluids exhibit quite different characteristics and are therefore discussed separately. For each fluid the heat flux is a function of two parameters. A convenient way to summarize the results is to

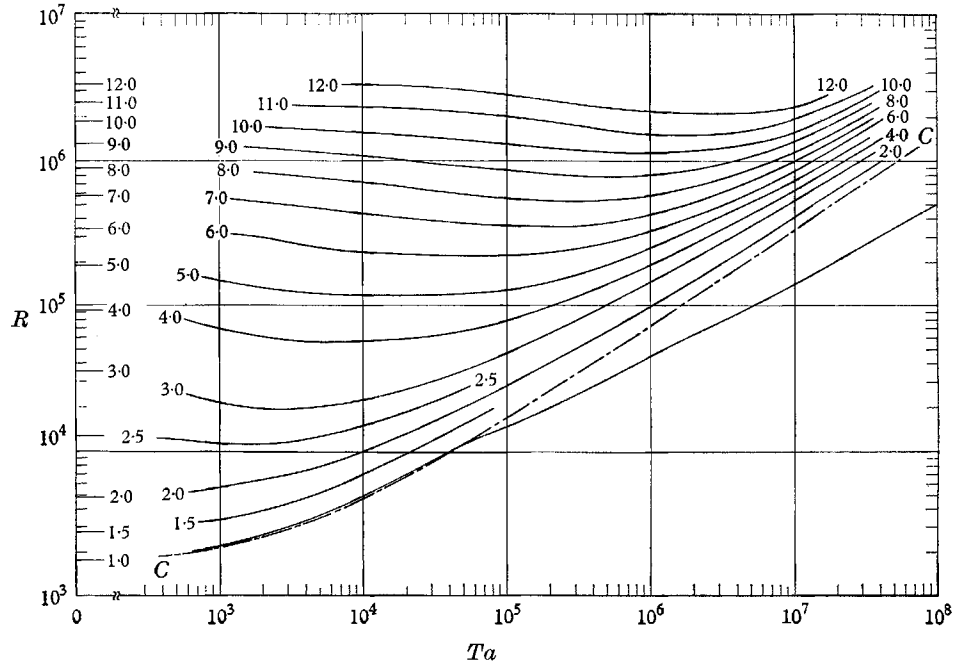

FIGURE 11. Lines of constant Nusselt number as a function of the Rayleigh and Taylor numbers in water with Prandtl number 6·8. Except for small values of the Nusselt number at large Taylor numbers the error in the Nusselt number is $\lesssim \pm 2\,\%$.

plot lines of constant Nusselt numbers on a log Rayleigh number/log Taylor number diagram (see figure 11). Because of the extreme compression of both parameters the values of individual points have not been plotted. The large number of measurements precludes their tabulation in this paper.† The Rayleigh and Nusselt number estimates (with one exception discussed below) are accurate to within $\pm 2\,\%$. The error in Taylor number is less than $3\,\%$.

Water

The dot-dashed line C–C in figure 11 is the marginal stability curve according to Chandrasekhar (1961). We find excellent agreement between theory and experiment for the critical Rayleigh number at all Taylor numbers less than 5×10^4; beyond this the fluid becomes unstable at lower Rayleigh numbers

† A listing of the measurements may be obtained from the Department of Geology and Geophysics, Massachusetts Institute of Technology, Cambridge, Massachusetts.

than the marginal stability theory predicts. At a Taylor number = 10^8, for example, the measured critical Rayleigh number is about one-third the expected value. We do not understand why this should be. It is found to be quite reproducible; i.e. if one changes the depth of the fluid, the instability will occur at the same Rayleigh number for a given Taylor number. It appears therefore to be a finite-amplitude instability, but we cannot entirely rule out the possibility that it is caused by the curvature of the hydrostatic pressure field in a rapidly rotating fluid. It will become evident below in the discussion of the

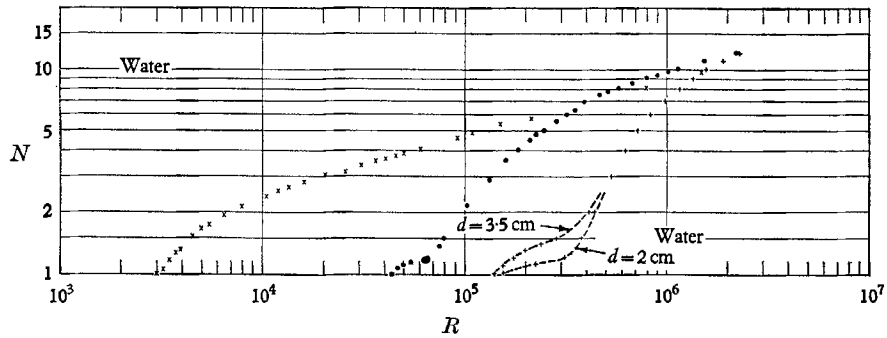

FIGURE 12. Cross-section of figure 11. The Nusselt number is plotted as a function of the Rayleigh number for three Taylor numbers: ×, $Ta = 3{\cdot}2 \times 10^3$; •, $Ta = 0{\cdot}95 \times 10^6$; +, $Ta = 10^7$.

mercury results that this instability is different from the one predicted by Veronis (1959, 1966). It can be easily verified that this subcritical instability cannot be an instability of the Ekman layer associated with a zonal flow.

However, the Nusselt numbers obtained for different spacings do not agree beyond the instability point until $N = 2{\cdot}5$ or larger. This is illustrated in figure 12, which is a cross-section of figure 11 at three different Taylor numbers. We note that at $Ta = 10^7$ there are two curves for the Nusselt number, depending on the depth. This discrepancy is due to the effects of the radial acceleration on the basic flow. For a given point in the diagram a smaller depth implies a higher rotation rate and a larger temperature drop, both of which co-operate to generate a stronger zonal circulation than at a larger depth. It is true that a larger temperature drop will also cause large convective velocities, but we show below that the ratio of zonal to convective motions will decrease with larger depths.

The Nusselt number can be written as

$$N = 1 + \frac{\langle wT \rangle}{R\Delta T/d}, \tag{5.1}$$

where $\langle\,\rangle$ denotes averaging over the whole layer (see Veronis 1959). From this we see that w, for a given Rayleigh number, is $\propto 1/d$ or $\propto \Delta T^{\frac{1}{2}}$. The zonal velocity can be obtained from the thermal wind equation, which gives us an approximate estimate

$$v_{\mathrm{rel}} = \tfrac{1}{4}\alpha\Omega R\Delta T, \tag{5.2}$$

which for constant Rayleigh and Taylor numbers is $\propto 1/d^2 d^3 = 1/d^5$.

The ratio of zonal to convective velocity is, then, proportional to d^{-4}, and consequently a large spacing is preferred. Because of the ambiguity in measurements near the critical Rayleigh number, we cannot be certain that even with the larger spacing we have obtained the correct values. For this reason we have not drawn any iso-Nusselt-number lines between $N = 1{\cdot}0$ and $N = 2{\cdot}0$. At larger Nusselt numbers, however, the agreement is satisfactory, although even for the line $N = 2$ we have relied on data from larger spacings for its (proper) location. The question remains, however, as to why the subcritical instability should appear in a consistent way as the depth is changed whereas the Nusselt number does not.

Another outstanding feature of figure 11 is the existence of a maximum Nusselt number at a non-zero rotation rate for a given Rayleigh number, provided that the latter is greater than about 10^4. For a given Nusselt number $\gtrsim 3$, the reduction of the Rayleigh number from its non-rotating value to its minimum is quite constant and equal to 0·6. The locus of the minima is $R \approx 206(Ta)^{0{\cdot}63}$.

What physical mechanism is responsible for this increase in the Nusselt number with increasing Taylor numbers? It would seem unlikely that an increased rotational constraint could provide a greater heat flux. Of course, one may speculate that this results from the basic parabolic pressure field. This appears to be very unlikely, however, since from (5.2) it is clear that the zonal velocities must be negligibly small, the mean interior gradient being much smaller than $\Delta T/d$. There is no objection to the larger heat flux *per se* for we know that if we had free instead of rigid boundaries in a non-rotating system the onset of convection would occur at a much lower Rayleigh number. Hence for all Rayleigh numbers greater than this the heat flux would be greater with free boundaries. Numerical computations by Herring (1963) indicate that the Nusselt number is more than twice as large with free boundaries.

At the Taylor numbers for which the Nusselt number is a maximum we have a slowly rotating system, by which we mean that the geostrophic *constraint* is not fully developed and is limited to interior flow away from the viscous boundary layers. But we have just shown that the viscous boundary layer imposes a great constraint on the heat flux. Then is it possible for the rotation to modify this boundary layer in such a way that a larger heat flux can be convected? We do not know the answer to this, but it can be noted that the scale of the Ekman layer, if there were one, would be the same as the scale of the thermal boundary layer at the Taylor number where the Nusselt number is maximum. For example, at $R = 10^5$, $Ta = 10^4$ the Ekman scale is $dTa^{-\frac{1}{4}}$ or $0{\cdot}1d$ and the the thermal boundary layer is $\frac{1}{2}d/N = 0{\cdot}12d$. This suggests that an Ekman layer like perturbation of the boundary layer may modify it in such a way that the thermal gradients are intensified with a correspondingly larger heat flux as a result. It is clear that as the rotation is further increased the Ekman-layer scale will be smaller than the thermal boundary layer, leaving the latter increasingly exposed to a geostrophic constraint. Hence the decrease in heat flux at very large Taylor numbers.

The rate of growth of the Nusselt number with Rayleigh number becomes

more rapid as the Taylor number is increased. It is tempting to speculate whether this approaches a limiting value or whether the Nusselt number would grow discontinuously if the Taylor number were increased without limit. It is worth observing that at these large Taylor and hence Rayleigh numbers there is at marginal stability an immense amount of potential energy stored in the fluid. Thus once a perturbation is allowed to grow there will be very large thermal gradients established, which may further enhance the instability. However, the measurement of such an integral property as the heat flux does not reveal the significant features of this process.

Mercury

Mercury responds quite differently from water to the effects of rotation, which we may expect because the small Prandtl number for mercury (0·025) will allow the possibility of time-dependent and finite-amplitude types of in-

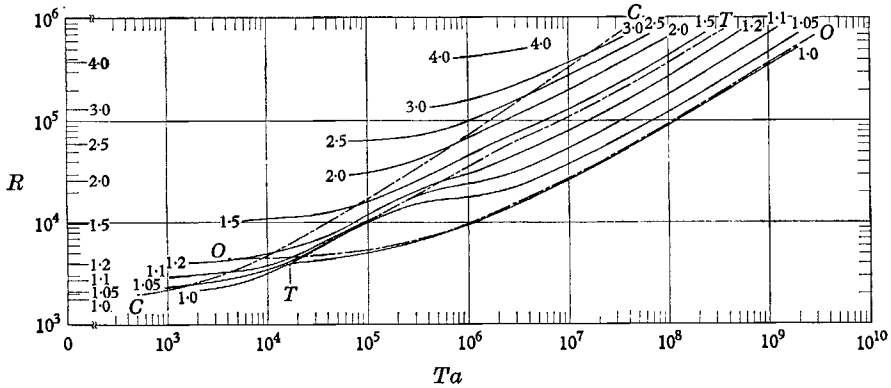

FIGURE 13. Lines of constant Nusselt number as a function of the Rayleigh and Taylor numbers in mercury with Prandtl number 0·025. The dot-dashed lines *O–O* and *C–C* are the marginal stability lines according to Chandrasekhar (1961) for oscillatory and steady convection. The dot-dashed line *T–T* delineates the experimentally determined transition between oscillatory and irregular convection. The error in the Nusselt number is $\lesssim \pm 3\%$.

stabilities. The curves *C–C* and *O–O* in figure 13 are the marginal stability curves for steady and oscillatory convection according to Chandrasekhar (1961). We find excellent agreement between experiment and theory when the Taylor number is greater than 10^5.

For Taylor numbers less than $1{\cdot}8 \times 10^4$ the agreement between linear theory and experiment is poor. This is expected because of a finite-amplitude instability which has been suggested by Veronis (1959, 1966). This instability, he argues, is based on the growth of a disturbance which will offset the effects of rotation in such a way that the convective flow can be maintained even when the Rayleigh number is reduced below its critical value (according to linear theory) for a given rotation rate. There are not yet available exact computations of the limiting curve for this instability with rigid boundaries, but the general form of the stability curve with free boundaries is very similar to our results. One specific difference, however, is that experimentally the flow is not steady.

For Taylor numbers between $1{\cdot}8 \times 10^4$ and 10^5 experiment and theory do not quite agree. In this range the onset of oscillatory convection must be established by studying the time recording of a thermocouple in the fluid to verify the presence of oscillatory temperature fluctuations (see figure 16). The convective heat fluxes are so small that the exact location of the critical Rayleigh number

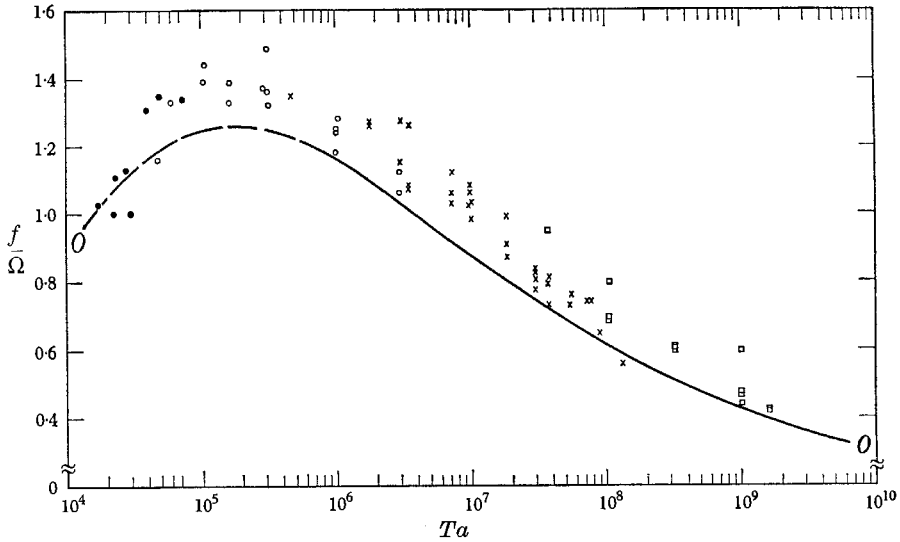

FIGURE 14. Experimentally determined values for the oscillation frequency for oscillatory convection in mercury as a function of the Taylor number for different depths of the fluid: ●, 0·69 cm; ○, 1·0 cm; ×, 1·8 cm; □, 3·0 cm. The line *O–O* is the oscillation frequency according to Chandrasekhar (1961). Its exact location is not known between $Ta = 10^4$ and $Ta = 10^6$.

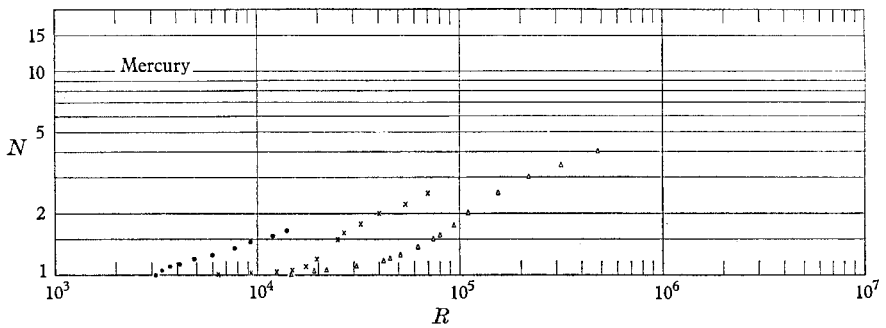

FIGURE 15. Cross-section of figure 13. The Nusselt number is plotted as a function of the Rayleigh number for three Taylor numbers: ●, $Ta = 10^4$; ×, $Ta = 3 \times 10^5$; △, $Ta = 3 \times 10^6$.

cannot be determined by extrapolation to $N = 1{\cdot}00$. We do not know with any certainty why the stability curve is about 10–15 % lower than the theoretically predicted curve. Since the discrepancy is much larger in this range of Taylor numbers than at larger Taylor numbers, we believe it is a characteristic of the fluid. It is possible that it is a finite-amplitude oscillatory instability. Some evidence of this may be found in figure 14, which shows the oscillation frequency as

a function of the Taylor number. The heavy line *O–O* is according to Chandrasekhar (1961) and is dashed between 10^4 and 10^6 because he did not report any values of the frequency in this range. Note that the data scatter on the upper side of the curve, as one might expect, since the frequency increases slightly with the Rayleigh number. However, for Taylor numbers between 10^4 and 4×10^4 the points scatter on the lower side of the curve and, in fact, the frequencies jump almost discontinuously at about $Ta = 4 \times 10^4$. This may be an indication of a different type of instability. It would be valuable to know the exact location of the oscillation frequency curve in this range.

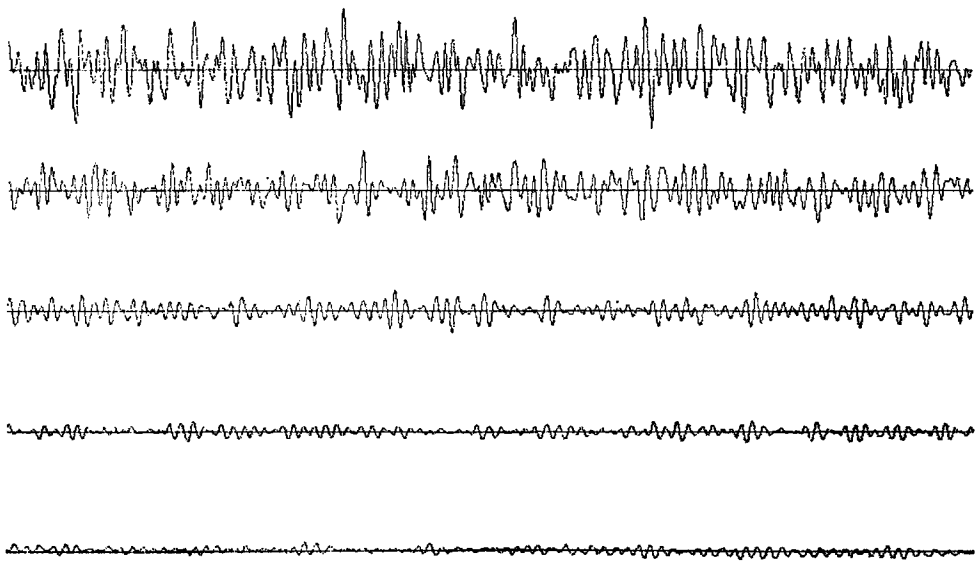

FIGURE 16. Sample records of the temperature fluctuations in mercury for increasing Rayleigh numbers at a Taylor number = $3{\cdot}8 \times 10^7$. The Rayleigh numbers are 72,000; 94,000; 126,000; 191,000 and 250,000. The three lower records are regarded as oscillatory and the upper two as irregular.

Although the finite-amplitude steady instability curve intersects the oscillatory instability curve at $Ta = 1{\cdot}7 \times 10^4$, it is still a clearly defined instability at Taylor numbers up to 10^5 and beyond, although the fluid is first unstable to the oscillatory instability.

For Taylor numbers greater than 10^6, in the asymptotic range, the transition Rayleigh number from oscillatory to irregular motion is about $4R_c Ta$ and is indicated by the dot-dashed curve *T–T* (see figure 13). It is somewhat vaguely defined as the highest Rayleigh number at which one can, without ambiguity, determine an oscillation frequency by a simple period count. At larger Rayleigh numbers periodic fluctuations still exist, but these are spread over a wide band of higher frequencies. Figure 16 shows a sample recording of such oscillations for increasing Rayleigh numbers. The three lower ones are regarded as oscillatory and the top two as irregular. A power spectrum analysis of these is given in figure 17, and clearly indicates considerable spreading in the spectrum for the two largest Rayleigh numbers.

The transition from oscillatory to irregular convection is accompanied by a more rapid rate of increase in heat flux with the Rayleigh number. Although the transition is not abrupt, it is clearly distinguishable in figure 15, which is a cross-section of figure 13 at $Ta = 10^4$, $Ta = 3\times10^5$ and $Ta = 3\times10^6$. Our results are inconsistent with those of Goroff (1960), who performed experiments

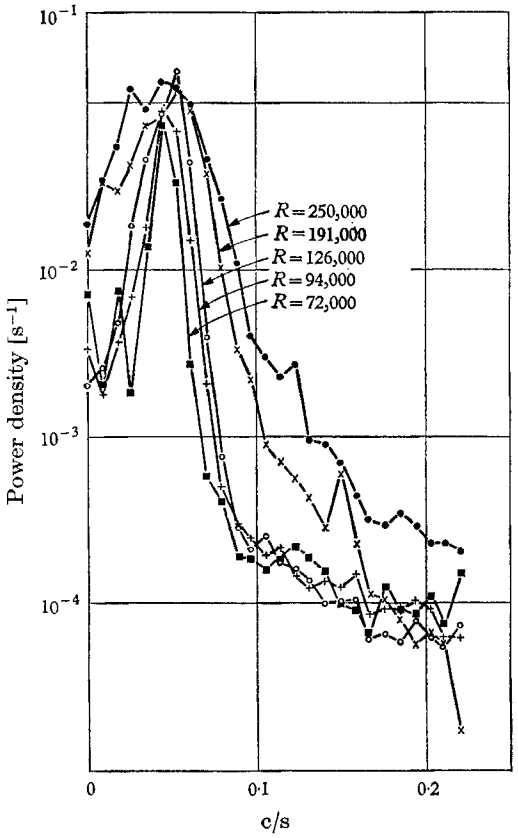

FIGURE 17. Power density spectrum of temperature oscillations in figure 16 at different Rayleigh numbers: □, R = 72,000; +, R = 94,000; ○, R = 126,000; ×, R = 191,000; ●, R = 250,000. The Taylor number is $3{\cdot}8\times10^7$.

in a rotating layer of mercury explicitly to establish whether oscillatory convection is preferred for *all* Rayleigh numbers less than the critical value for steady convection. His results indicated that this was the case, whereas we find the transition to occur at a significantly lower Rayleigh number. It is not clear why our results should disagree so completely. We also note that his values for the Nusselt number are generally much smaller than those presented here.

6. Summary

This study has led to a more precise description of the stability properties of Bénard convection over a wide range in Taylor numbers at the two Prandtl numbers corresponding to water and mercury. In both cases we have found

partial confirmation of the linear stability theory for the onset of steady and oscillatory convection.

Measurements with water revealed two striking features. The first is the presence of a subcritical instability at Taylor numbers greater than 5×10^4 which becomes more pronounced at larger Taylor numbers. There is, however, some uncertainty about the accuracy of this observation due to the fact that the parabolic pressure field in a rotating system creates an undesired zonal flow which is not entirely negligible where this instability occurs. This is particularly noticeable in the heat flux measurements at Rayleigh numbers slightly larger than the observed critical value.

The second feature is that water exhibits a maximum heat flux not without rotation but at a Taylor number which is an increasing function of the Rayleigh number, $Ta = 206(Ta)^{0.63}$. It was conjectured that this increase is due to an 'Ekman-layer-like' modification of the viscous boundary layer. If this is true, one should not observe a similar increase with free boundary conditions. As the Taylor number for a given Rayleigh number is increased even further, however, the heat flux is rapidly reduced until the convection is suppressed entirely.

Mercury has quite different characteristics. There is strong evidence of a finite-amplitude instability for $0 < Ta < 1{\cdot}8 \times 10^4$, which is in good qualitative agreement with a theoretical prediction by Veronis (1966). There is also evidence of a finite-amplitude oscillatory instability over a limited range in the Taylor number $1{\cdot}8 \times 10^4 < Ta \lesssim 10^5$. This was established by the presence of temperature oscillations at a slightly subcritical Rayleigh number with a lower frequency than expected by linear theory. For all Taylor numbers greater than 10^5 the experiments are in excellent agreement with the predictions of the linear stability theory regarding the critical Rayleigh number and the oscillation frequency. In mercury the Nusselt number is a monotonically decreasing function of the Taylor number. Further, it is much smaller than in water for any value of the Rayleigh and Taylor numbers except, of course, where mercury is unstable and water is not. There was no Taylor number at which water was unstable and mercury stable.

Heat flux measurements with mercury, water and also a silicone oil with a Prandtl number 200 were made without rotation. With water and the silicone oil we have found good agreement with earlier measurements by Silveston (1958). The Nusselt number for the oil can be written $N = 0{\cdot}184R^{0.281}$ for $R > 4000$. The upper limit is not known. Water follows this relation closely for $R < 7000$. At larger Rayleigh numbers non-linear dynamical effects due to the smaller Prandtl number become important and a better relation is given by $N = 0{\cdot}131R^{0.30}$. Again the upper limit is not known.

Mercury yields much lower Nusselt numbers and can be approximated $N = 0{\cdot}147R^{0.257}$ for $R > 20{,}000$. It is significant that no steady flow was ever observed with mercury. The accuracy of the heat flux measurements excludes the possibility of expressing the Nusselt number as constant $\times R^{\frac{1}{3}}$ over the range of Rayleigh numbers considered here.

A limited number of visual observations of the convective motions with rotation were made. The principal feature as the rotation was increased was first

the horizontal buckling of the convective rolls and finally their complete breakdown into vortices in what appeared to be a random distribution.

I wish to express my gratitude to Prof. R. Hide for the opportunity to undertake this study. His encouragement and support was deeply appreciated. I also want to thank Prof. G. Veronis and Prof. T. Madden for many stimulating discussions. This study was supported by the National Science Foundation under Grant NSF G22390. Support from the Office of Naval Research, under Grant Nonr 1841(74), is also gratefully acknowledged.

Appendix A. Computation of the heat flux

The state of the experiment is for our purposes completely given by T_{32}, T_{41} (see figure 1) and T_{mean}, where T_{32} specifies the temperature difference across the fluid, $(T_{41}-T_{32})$ is a measure of the heat flux and T_{mean} is essentially the average temperature of the fluid. The electrical output of the thermocouples is measured by a Leeds and Northrup potentiometer, type K-3, with a resolution of $\sim 0{\cdot}1\ \mu$V. When the experiment has reached steady-state conditions, the measurements are carried out in the following order: (i) check null position with a low-resistance (short) circuit going through the slip rings and all connectors. This is to make sure that no spurious e.m.f. is present in the plugs or slip rings. The maximum error ever observed is $-0{\cdot}3\ \mu$V; (ii) check calibration of potentiometer with standard cell; (iii) measure T_{32} in μV; (iv) measure T_{41} in μV; (v) measure T_{mean} in μV; (vi) measure T_{32} in μV.

Unless steps (iii) and (vi) agree and do not change, the set is not accepted. In practice, a large heat flux by turbulent convection can cause T_{32} to vary slightly, $\pm 0{\cdot}1$ to $\pm 0{\cdot}5\,\%$, depending on the fluid and the degree of turbulence, in which case an average is estimated.

The computation of the heat flux is based on the assumption that the flux is the same in both epoxy layers and in the fluid (including the plexiglass wall). This is probably not exactly true, particularly if the ambient temperature differs from T_{mean} and if the fluid layer is thick. However, the experiment is reasonably well insulated all around with at least a 1 in. thick padding of cotton, and T_{mean} is maintained to within $\pm 1{\cdot}5$ °C of room temperature and practically all measurements. Thus the assumption above is considered to be valid. The heat flux per unit area through the epoxy layer is then simply

$$H_1 = (k_F/2l_F)\,(T_{41}-T_{32}), \tag{A 1}$$

where k_F and l_F are the thermal conductivity and thickness of each epoxy layer and H_1 is the heat flux per unit area, where T_{32} and T_{41} have been converted from μV to degrees Celsius.

The total heat flux through the epoxy layer is equated to the sum of the heat fluxes in the fluid, area A_2, and the plexiglass wall, area A_3:

$$H_1 A_F = H_2 A_2 + (k_p T_{32}/d) A_3, \tag{A 2}$$

where H_2 is the corrected heat flux in the fluid per unit area, k_p is the conductivity of the plexiglass and A_F the area of the epoxy layers. Given the dimensions

and the conductivities k_F and k_p, the heat flux H_2 is known once T_{32} and T_{41} are measured. Actually, k_F is not known *a priori*. It is determined, instead, by measuring the heat flux under non-convecting conditions. This is done most simply by setting the apparatus upside down and heating from above so that a stable stratification of the fluid results, or by rotating the experiment rapidly so that the convection is inhibited.

The heat flux in the fluid is then

$$H_2 = kT_{32}/d, \tag{A 3}$$

where k is the thermal conductivity of the fluid. Combining this with (A 1) and (A 2), we obtain the heat meter constant, C_1:

$$C_1 = \frac{k_F}{2l_F} = \frac{kA_2 + k_p A_3}{d(T_{41}/T_{32} - 1)A_F}. \tag{A 4}$$

In some of the heat flux measurements in water the output of the thermopile T_{32} was partially shorted ($\sim 10\,\%$). This was not noticed at first. Fortunately the experiment had been calibrated at each depth (a determination of C_1 in equation (A 4). After the circuitry was repaired a new determination of C_1 was performed and the error in C_1 was attributed to an error in T_{32}. The loss in accuracy of T_{32} due to this mishap is *at worst* $\lesssim 0{\cdot}3\,\%$.

A more serious error became evident when about half of the water experiments were completed. C_1 was not constant but appeared to increase linearly as the depth was reduced. This was brought about by an unsatisfactory thermal contact between the thermocouples and the copper plates. The thermocouple wires are wrapped around the aluminium blocks before they enter the holes on the side of the copper plates. Hence gradients existed in the wires and introduced an error which was proportional to the temperature difference between the aluminium block and the copper plates. This difficulty was remedied by improving the thermal contact between the thermocouples and the copper plates by adding an aluminium oxide powder to the contact compound. Thereafter the experiment was calibrated anew. The new values for C_1 approached an asymptotic value as the depth was decreased. The change in C_1 resulting from this correction was used to correct T_{32} (see (A 4)). The loss of accuracy from this correction is estimated to be less than $0{\cdot}2\,\%$.

Nevertheless, after these corrections had been cared for with water, C_1 still decreased from its asymptotic value by $\sim 3\,\%$ as the depth increased from 0·5 to 3·5 cm. With a 20 cSt silicone oil C_1 varied by about 11%. With mercury a measurable trend could not be established. This variation originates from an increased contribution to the heat flux by the cotton insulation just outside the side walls as the depth is increased and becomes relatively larger as the conductivity of the fluid is decreased. This decrease in C_1 can be attributed to a failure to estimate the $k_p A_3$ term properly; hence we have in effect an accurate correction for these side wall effects. Thus, for each depth, $k_p A_3$ is modified by a correction factor in such a way that C_1 is maintained constant.

Very large heat fluxes give rise to non-negligible gradients in the copper plates between the thermocouples and the metal–fluid interfaces, in which case the

measured temperature drop must be corrected in order to yield the true temperature drop across the fluid. The measured temperature, T_{32}, is the sum of the temperature drops in the metal of thickness d cm and across the fluid, T_M and T'_{32}, say:

$$T_{32} = T'_{32} + T_M. \tag{A 5}$$

The requirement that the heat flux is constant through the fluid and the copper plates gives us

$$A_F \frac{k_{cu} T_M}{d_{cu}} = \frac{k T'_{32} N_p}{d} A_2, \tag{A 6}$$

where d is the fluid depth. By eliminating T_M between (A 5) and (A 6) we have

$$T'_{32} = T_{32} \Big/ \left[1 + \frac{d'_{cu} k N A_2}{k_{cu} d A_F} \right]; \tag{A 7}$$

k is the conductivity of the fluid and N is the Nusselt number, which is defined as the ratio of the actual heat flux in the fluid divided by the heat flux that would take place by conduction alone. Hence kN is the effective conductivity of the fluid and T'_{32} is the corrected temperature difference across the fluid. Because we have redefined T_{32}, we must modify the constant C_1 so that they are consistent. We do this by setting $N = 1$ in (A 7) and replacing T_{32} with T'_{32} in (A 4).

A first estimate of the Nusselt number which is required to compute T'_{32} in (A 7) is obtained by eliminating H_1 between (A 1) and (A 2). We have

$$C_1(T_{41} - T_{32}) A_F = H_2 A_2 + \frac{k_p T_{32}}{d} A_3 \tag{A 8}$$

or

$$H_2 = C_1(T_{41} - T_{32}) \frac{A_F}{A_2} - \frac{k_p T_{32}}{d} \frac{A_3}{A_2}, \tag{A 9}$$

where H_2 is computed using the uncorrected value T_{32}. The Nusselt number is then obtained by dividing the actual heat flux by the flux that would take place in the absence of convection, or

$$N = H_2 \Big/ \frac{k T_{32}}{d}. \tag{A 10}$$

This first estimate of N is inserted into (A 7) to obtain the corrected value T'_{32}. H_2 and N are then recomputed with T'_{32} instead.

T'_{32}, H_2 and N give our best estimates of the temperature drop and the heat flux. It is convenient, however, to present T'_{32} in non-dimensional form as the Rayleigh number

$$R = \alpha g T'_{32} d^3 / \nu \kappa, \tag{A 11}$$

where α, ν and κ in general are functions of T_{mean}.

The data are punched on to cards, one per measurement, and processed as outlined above on a computer. The physical properties of the fluid are computed by a sub-program where α, ν, κ and k are given as algebraic functions of T_{mean}. Their values as a function of temperature are listed in appendix B.

The thermo-electric power of the thermocouples is assumed to obey the relation

$$\text{e.m.f. } \mu\text{V/degC} = A + \epsilon(T_{\text{mean}} - 22), \tag{A 12}$$

where $A = 39{\cdot}97\,\mu\text{V/°C}$ and $\epsilon = 0{\cdot}09$. A is calibrated by maintaining the aluminium blocks at a constant and accurately known temperature difference with negligible heat flux, to avoid any gradients, and measuring T_{41}. This calibration is required because the thermocouples are guaranteed only to 1 % accuracy by the manufacturer. ϵ is obtained from *International Critical Tables* (1928).

Appendix B. A tabulation of the physical properties of mercury, water and silicone oils

A detailed tabulation is presented of the physical properties of mercury, water and 20 cSt silicone oil as a function of temperature. These properties include the density ρ (g/cm^3), the coefficient of thermal expansion α (°C^{-1}), the kinematic viscosity ν (cm^2/sec), the dynamic viscosity η (g/cm sec), the thermal conductivity k (cal/cm °C sec), the heat capacity C (cal/g °C), the thermal diffusivity κ (cm^2 sec^{-1}) and the Prandtl number $P\,(= \nu/\kappa)$. In addi tion, a less detailed listing of the properties of silicone oils is given for a wide range of temperatures.

Mercury (table 6)

The data are taken exclusively from the *Liquid Metals Handbook* (1953). This is in itself a collection of different sources of data and also includes a commentary on the original sources and the probable accuracies. We point out that there is a large discrepancy (~ 30 %) between different sources on the thermal conductivities.

Water (table 7)

The density, dynamic viscosity and thermal conductivity are taken from *International Critical Tables* (1928). The specific heat is taken from *Tables of Physical and Chemical Constants* (1959).

20 centistoke silicone oil (table 8)

The density and the coefficient of expansion are taken from Bulletin no. 05-061 (Dow Corning Chemical Products Division 1963). The value for the heat capacity was suggested to me by Dr A. Ingersoll (1965). The kinematic viscosity is measured experimentally, as the values given by the manufacturer are only nominal. The thermal conductivity is also measured experimentally and is 1 % smaller than that given by the manufacturer. Our value is used.

Dow Corning silicone fluid no. 200 (table 9)

This table is a reduced version of Bulletin no. 05-061 (Dow Corning Chemical Products Division 1963). The heat capacity data were suggested to me by Dr A. Ingersoll (1965). The density, coefficient of expansion, kinematic viscosity and thermal conductivity are taken from Bulletin no. 05-061. The dynamic viscosity, thermal diffusivity and the Prandtl number are computed from the preceding properties.

T	ρ	$\alpha \times 10^3$	$\eta \times 10^2$	$\nu \times 10^3$	$k \times 10$	$C \times 10$	$\kappa \times 10$	$P \times 10$
20	13·55	0·181	1·550	1·144	0·208	0·3321	0·463	0·247
21	13·54	0·181	1·544	1·140	0·209	0·3321	0·464	0·246
22	13·54	0·181	1·538	1·136	0·209	0·3320	0·466	0·244
23	13·54	0·181	1·532	1·132	0·210	0·3319	0·467	0·242
24	13·54	0·181	1·526	1·127	0·211	0·3319	0·469	0·241
25	13·53	0·181	1·520	1·123	0·211	0·3318	0·470	0·239

TABLE 6. The physical properties of mercury as a function of temperature

T	ρ	$\alpha \times 10^3$	$\eta \times 10^2$	$\nu \times 10^2$	$k \times 10^3$	C	$\kappa \times 10^3$	P
20	0·9982	0·207	1·006	1·008	1·402	0·9991	1·406	7·17
21	0·9980	0·217	0·983	0·985	1·406	0·9989	1·410	6·99
22	0·9978	0·227	0·961	0·963	1·410	0·9988	1·415	6·81
23	0·9976	0·237	0·938	0·941	1·414	0·9987	1·419	6·63
24	0·9973	0·247	0·916	0·918	1·418	0·9986	1·424	6·45
25	0·9971	0·257	0·894	0·896	1·422	0·9985	1·428	6·28

TABLE 7. The physical properties of water as a function of temperature

T	ρ	$\alpha \times 10^3$	η	ν	$k \times 10^3$	C	$\kappa \times 10^3$	P
20	0·9603	1·07	0·2053	0·2137	0·337	0·346	1·014	211
21	0·9593	1·07	0·2006	0·2091	0·337	0·346	1·015	206
22	0·9582	1·07	0·1959	0·2044	0·337	0·346	1·016	201
23	0·9571	1·07	0·1912	0·1997	0·337	0·346	1·018	196
24	0·9561	1·07	0·1865	0·1951	0·337	0·346	1·019	192
25	0·9550	1·07	0·1818	0·1904	0·337	0·346	1·020	187

TABLE 8. The physical properties of 20 cSt silicone oil as a function of temperature

$\nu \times 10^2$	ρ	$\alpha \times 10^3$	$k \times 10^3$	C	$\kappa \times 10^3$	P
1	0·818	1·34	0·24	0·435	0·674	14·8
2	0·873	1·17	0·26	0·402	0·741	27
3	0·900	1·06	0·27	0·386	0·780	38·5
5	0·920	1·05	0·28	0·37	0·824	61
10	0·940	1·08	0·32	0·356	0·955	105
20	0·955	1·07	0·34	0·346	1·03	194
100	0·968	0·96	0·37	0·335	1·14	877

TABLE 9. Typical properties of Dow Corning silicone fluid no. 200 at 25 °C

REFERENCES

BUSSE, F. 1966 Unpublished manuscript.

CHANDRASEKHAR, S. 1961 *Hydrodynamic and Hydromagnetic Stability.* Oxford University Press.

DOW CORNING, Chemical Products Division, 1963 Bulletin no. 05-061.

FOWLIS, W. W. & HIDE, R. 1965 Thermal convection in a rotating annulus of liquid: effect of viscosity on the transition between axisymmetric and non-axisymmetric flow régimes. *J. Atmos. Sci.* **22**, 541–58.

FULTZ, D. & NAKAGAWA, Y. 1955 Experiments on over-stable thermal convection in mercury. *Proc. Roy. Soc.* A **231**, 211–25.

GLOBE, S. & DROPKIN, D. 1959 Natural convection heat transfer in liquids confined by two horizontal plates and heated from below. *J. Heat Transfer*, **81**, 24–8.

GOROFF, I. R. 1960 An experiment on heat transfer by over-stable and ordinary convection. *Proc. Roy. Soc.* A **254**, 537–41.

HERRING, J. R. 1963 Investigations of problems in thermal convection. *J. Atmos. Sci.* **20**, 325–38.

INGERSOLL, A. P. 1965 Ph.D. Thesis, Harvard University.

International Critical Tables 1928 New York: Wiley.

KOSHMIEDER, E. L. 1966 On convection on a uniformly heated plane. *Beit. Phys. Atmos.* **39**, 1.

Liquid Metals Handbook 1953 Washington, D.C.: U.S. Government Printing Office.

MALKUS, W. V. R. 1954 Discrete transitions in turbulent convection. *Proc. Roy. Soc.* A **225**, 185–95.

MULL, W. & REIHER, H. 1930 Der Wärmeschutz von Luftschichten. *Beih. Gesundh. Ing.* Ser. 1, 28.

NAKAGAWA, Y. & FRENZEN, P. 1955 A theoretical and experimental study of cellular convection in rotating fluids. *Tellus*, **7**, 1–21.

NIILER, P. P. & BISSHOPP, F. E. 1965 On the influence of the Coriolis force on the onset of thermal convection. *J. Fluid Mech.* **22**, 753–61.

SCHMIDT, R. J. & MILVERTON, S. W. 1935 On the instability of a fluid when heated from below. *Proc. Roy. Soc.* A **152**, 586–94.

SCHMIDT, R. J. & SAUNDERS, D. A. 1938 On the motion of a fluid heated from below. *Proc. Roy. Soc.* A **165**, 216–28.

SILVESTON, P. L. 1958 Wärmedurchgang in Waagerechten Flüssigkeitsschichten. *Forsch. Ing. Wes.* **24**, 59–69.

SPIEGEL, E. A. & VERONIS, G. 1960 On the Boussinesq approximation for a compressible fluid. *Astrophys. J.* **131**, 442–7.

Tables of Physical and Chemical Constants 1959 12th edition. Longmans.

VERONIS, G. 1959 Cellular convection with finite amplitude in a rotating fluid. *J. Fluid Mech.* **5**, 401–35.

VERONIS, G. 1966 Motions at subcritical values of the Rayleigh number in a rotating fluid. *J. Fluid Mech.* **24**, 545–54.

WEISS, N. O. 1964 Convection in the presence of restraints. *Phil. Trans.* A **256**, 99–147.

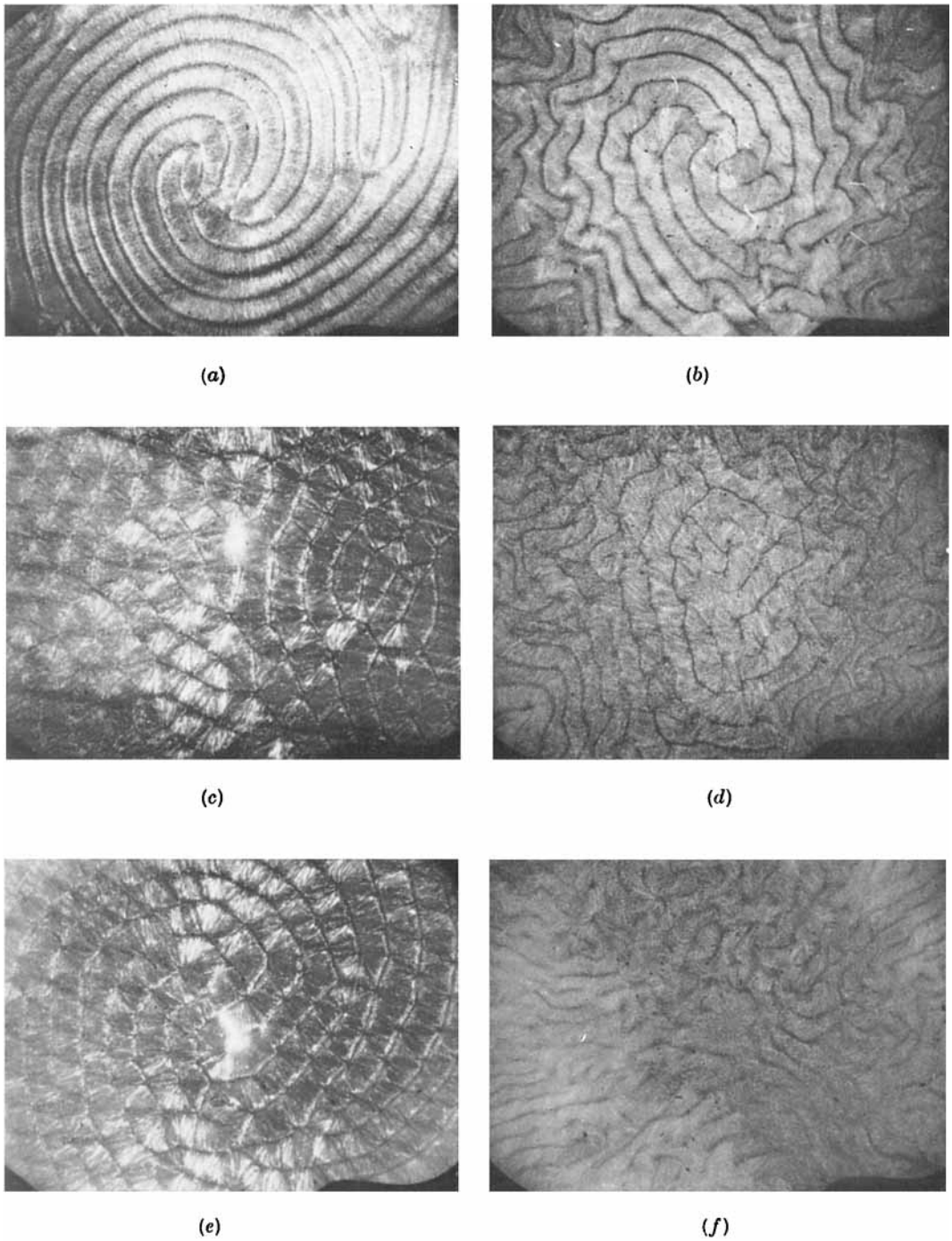

FIGURE 4. Vertical view of thermal convection for different values of the Rayleigh and Taylor numbers. $P = 100$. The depth of the fluid is 0·7 cm and the field of view is about 15 cm. The axis of rotation is at the centre of the photographs in this and the following two figures.

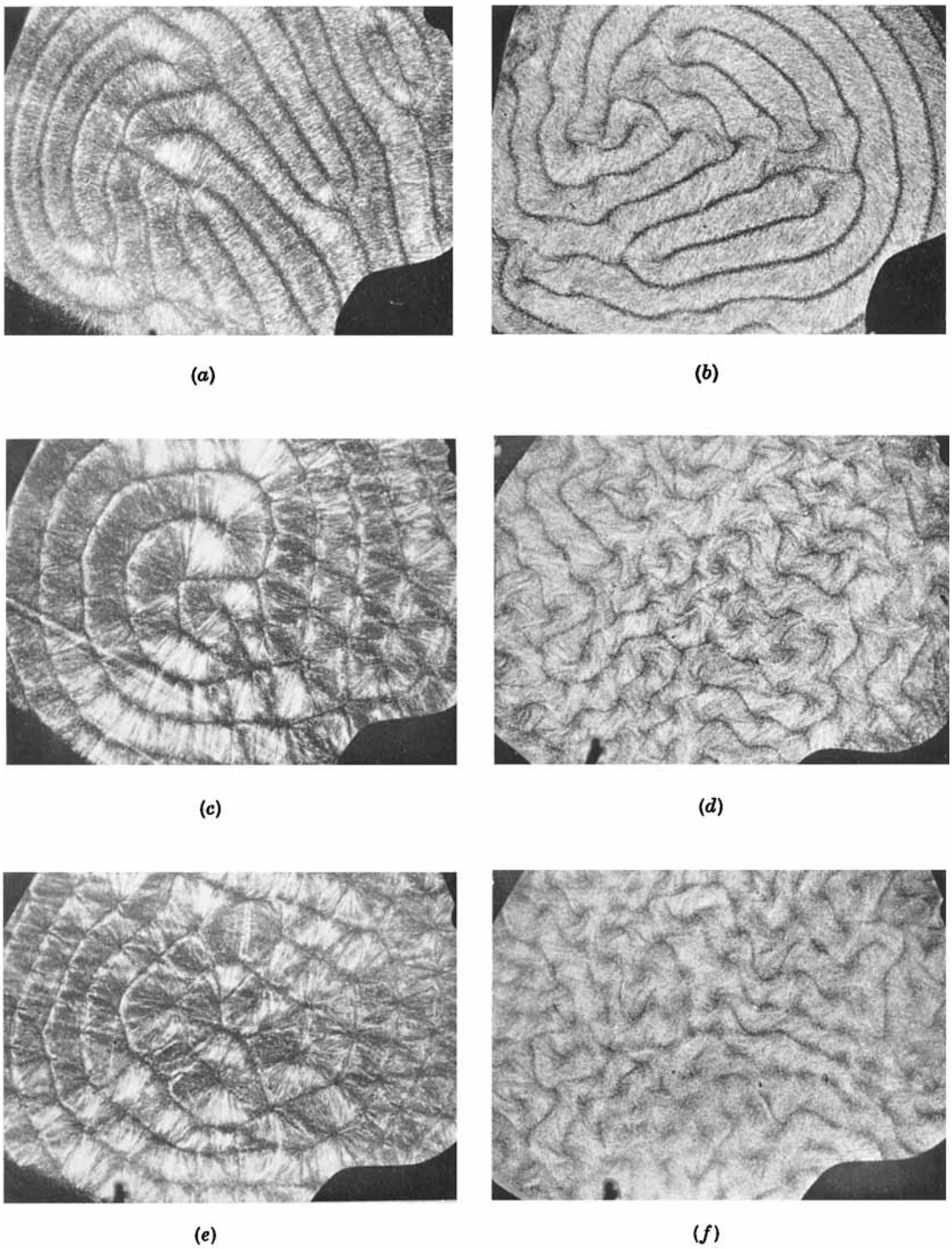

FIGURE 5. Vertical view of thermal convection for different values of the Rayleigh and Taylor numbers. $P = 100$. The depth of the fluid is 1·0 cm and the field of view is about 15 cm.

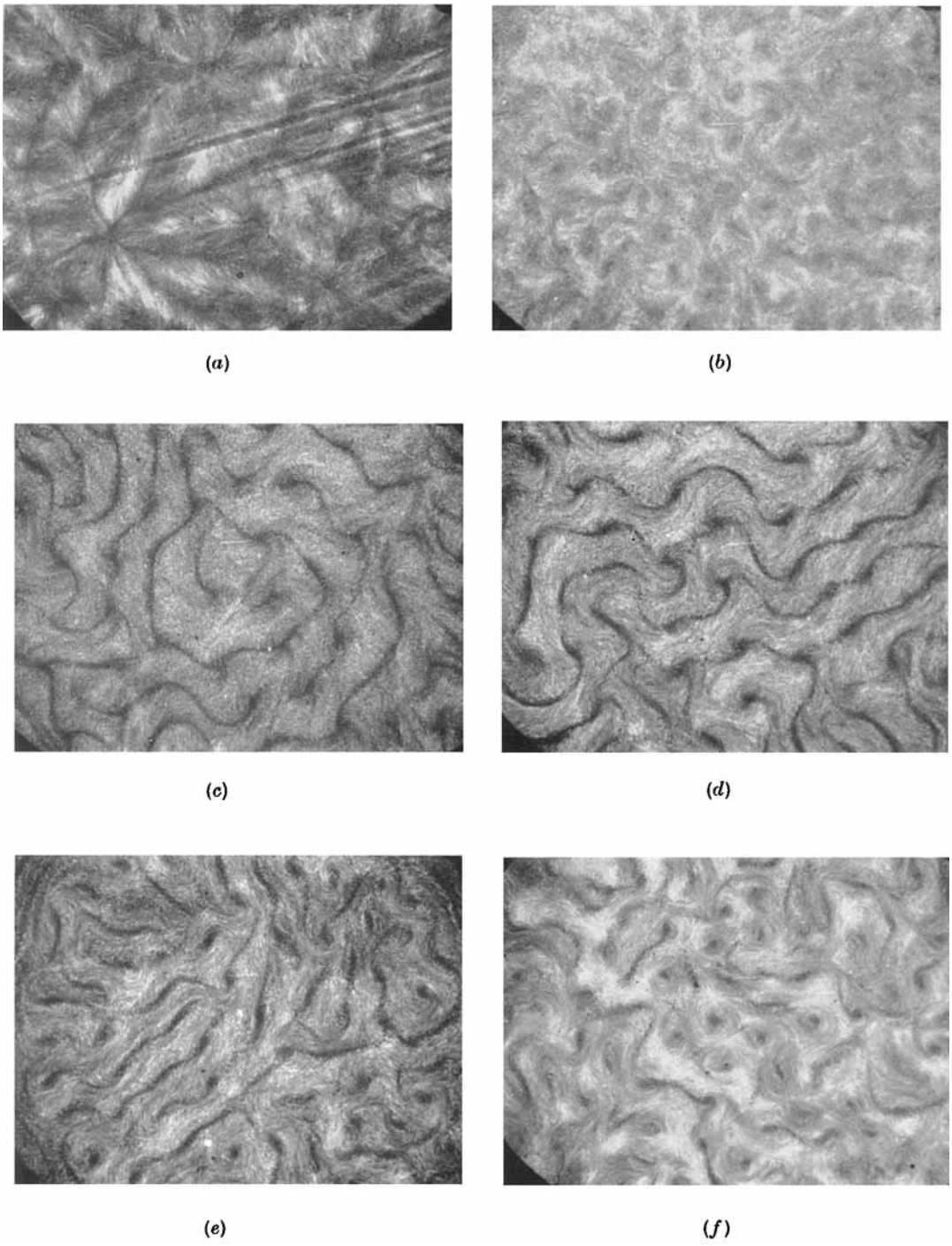

FIGURE 6. Vertical view of thermal convection for different values of the Rayleigh and Taylor numbers. $P = 100$. The depth of the fluid is 1·8 cm and the field of view is about 15 cm.